Kovove Mater. 59 2021 209–215
DOI: 10.4149/km_2021_4_209

Accumulative roll-bonding of aluminium sheets at room and cryogenic temperatures

M. Karlík[1,2]*, P. Homola[2,3], P. Sláma[4]

[1] *Charles University, Department of Physics of Materials, Ke Karlovu 5, 121 16 Prague 2, Czech Republic*
[2] *Czech Technical University in Prague, Faculty of Nuclear Sciences and Physical Engineering, Department of Materials, Trojanova 13, 120 00 Prague 2, Czech Republic*
[3] *Czech Aerospace Research Centre, Beranových 130, 199 05 Prague – Letňany, Czech Republic*
[4] *COMTES FHT a.s., Průmyslová 995, 334 41 Dobřany, Czech Republic*

Received 15 May 2021, received in revised form 23 July 2021, accepted 11 August 2021

Abstract

2 mm thick pure aluminium sheets (99.99 % Al) were processed by accumulative roll-bonding (ARB) at room temperature (RT) and under cryogenic conditions (CC, –196 °C). Their microstructure was characterized by means of electron backscattered diffraction (EBSD) and transmission electron microscopy (TEM), mechanical properties were examined by hardness measurements. Nearly equiaxed subgrains with a relatively high dislocation density in their interior were observed after the 1st ARB cycle. The following cycles result in subgrain flattening and reduction of inner dislocation density by recovery. The distribution of misorientations of the grain boundaries in CC and RT samples does not differ significantly; only the CC sample has a little higher fraction of the low-angle grain boundaries (LAGB) with misorientation 2°–5° at the expense of LAGB (5°–15°). The hardness increases vitally only during the first ARB cycle at RT; a slight decrease is even observed starting from the 2nd ARB cycle. During processing at CC, this decrease is shifted to the 4th cycle due to reduced post-dynamic recovery at low temperatures.

K e y w o r d s: accumulative roll-bonding, 99.99 % Al, electron microscopy, hardness

1. Introduction

A traditional objective of materials research is to develop strong materials. A suitable strength improvement without compromising ductility can be achieved by refinement in grain size [1, 2], introducing high-angle grain boundaries (HAGB) as substantial obstacles for dislocation glide. Conventional thermomechanical treatments lead to the grain size reduction to a few micrometers only [3], and so attention has been focused on the development of new techniques to produce materials with grain size in an ultrafine range (between 100 nm and 1 μm) or even a nano-range (less than 100 nm). Two methods, 'bottom-up' and 'top-down', have been used to prepare these materials [4]. In the 'bottom-up' approach, ultrafine-grained (UFG) materials are fabricated by physical or chemical methods from individual atoms or nanoparticles [5, 6]. However, these techniques are limited to the production of small samples which are not appropriate for structural applications. On the other hand, the 'top-down' approach starts from a bulk metal with relatively coarse grain size and UFG microstructure is achieved by severe plastic deformation (SPD) during high-pressure torsion (HPT) [7], equal channel angular pressing (ECAP) [8], constrained groove pressing (CGP) [9] or accumulative roll-bonding (ARB) [10]. ARB uses standard metalworking rolling mills; it consists of bonding two stacked sheets by rolling, sectioning the bonded strip in two halves, stacking them together again, and further rolling while maintaining the original sheet thickness. During ARB processing, the original grains are progressively segmented by new boundaries induced by deformation, and uniform nanostructures are formed after multiple ARB passes. This deformation-induced grain fragmentation is often

*Corresponding author: tel.: +420 224358507; fax: +420 224358523; e-mail address: Miroslav.Karlik@fjfi.cvut.cz

accompanied by softening the material by recovery. The final microstructure of ARB processed materials thus depends not only on deformation factors (deformation temperature, strain level, strain rate, symmetry of rolling [11]) but also on materials factors, including initial grain size, presence of solute atoms, or second phase particles in the matrix, or stacking fault energy [12]. ARB processing has been successfully applied at room and elevated temperatures to various kinds of alloys [13] or nano-grained multi-layered metallic composites [14–17]. ARB processing of pure aluminium was reported already by several authors [15, 16, 18–22]. Rahmatabadi et al. [15, 16] focused on the plane stress fracture toughness or forming limit diagrams of the ARB AA1050 (99.5 % Al), Delshad Golami et al. [18] studied forming limit diagrams and mechanical properties of the same material. Ivanov and Ovcharenko [19] used Al of lower purity (99.17 % Al) and compared the properties of samples processed by ARB and ECAP. Su et al. [20] reported the evolution of the microstructure and mechanical properties of AA1050 (99.5 % Al). Kamikawa et al. [12] performed a systematic ARB study on various degrees of aluminium purity (99.2, 99.99, and 99.999 % Al). Wang et al. [21] studied microstructure, texture, and mechanical properties of AA1060 (99.6 % Al) ARB processed in cryogenic conditions.

In the present work, ARB processing in cryogenic conditions is applied to higher purity aluminium (99.99 %) than in [21] to investigate hardening and microstructure without the presence of solute atoms. Furthermore, the microstructure and mechanical properties of the sheets are compared to the same material ARB processed at room temperature.

2. Experimental details

A direct-chill (DC) cast and hot-rolled 9.0 mm plate of pure aluminium (99.99 wt.%) was cold-rolled down to the thickness of 2.0 mm (reduction of 78 %). A fully recrystallized sheet was prepared by annealing for 30 min at 350 ℃. ARB processing consisted of the repetition of the following steps: (1) degreasing in tetra-chloroethylene and wire-brushing with stainless steel 0.3 mm wire brush; (2) stacking of two pieces of $300 \times 50 \times 2\,\mathrm{mm}^3$; (3) joining by Al wires; (4) cooling in liquid nitrogen (optional); (5) rolling without lubricant to 50 % reduction in thickness. Roll diameter of 340 mm and peripheral speed of $30\,\mathrm{m\ min}^{-1}$ were used. In order to prevent the propagation of edge cracks, specimen edges were trimmed and smoothed down. Rolling at cryogenic conditions (CC) was performed after soaking the Al sheet stack in the liquid nitrogen (−196 ℃) for 10 minutes. The temperature of the sheet after rolling was −26 ℃, as determined by an infrared thermometer. After room-temperature (RT) ARB processing, the sheet temperature increased to 107 ℃. At first, RT processing was performed up to six ARB cycles. The CC processing followed, but it was stopped already after four ARB cycles because the hardness of the sheet started to decrease. We did not want to continue performing complicated processing without improving the mechanical properties of the sheet. HV10 measurements (nominal loading force 98.07 N) were performed on the surface of the sheets, i.e., in the rolling (long-transverse, L-T) plane, according to standard CSN EN ISO 6507–1. Average values and standard deviations were determined from at least seven indentations. The grain structure of the samples was examined on sections in the L-T plane using an EDAX Trident electron backscattered diffraction (EBSD) system mounted on FEI Quanta 200 FEG scanning electron microscope (SEM) equipped with a Schottky field-emission gun. Samples for EBSD were prepared by mechanical grinding, diamond emulsion polishing down to 1 μm, and final polishing using colloidal SiO_2 water solution (Buehler Mastermet 2). Transmission electron microscopy (TEM) foils were prepared from 3 mm × 2 mm strips in size cut in the long-short (L-S) plane. After mechanical grinding to 0.15 mm, the strips were electrolytically twin-jet polished (−30 ℃, 30 V) in Struers Tenupol 5 unit filled with 30 % HNO_3 solution in methanol. During electrolytic polishing, the samples were protected from both sides by platinum masks with holes 1.6 mm in diameter. Obtained thin foils were observed at 200 kV acceleration voltage using JEOL JEM 2000FX microscope equipped with an energy dispersive spectrometer Bruker and CCD camera Veleta.

3. Results and discussion

3.1. Hardness

The results of the ARB processing at room temperature (RT) showed that a significant increase of the hardness (nearly 3 times) is observed only after the first ARB cycle, and the following cycles are accompanied even by slight softening of the material (Fig. 1). Cryo-ARB processing aimed to study the influence of extremely low temperatures (–196 ℃) on the stability of the hardening of the aluminium sheet material. The evolution of hardness in cryogenic conditions (CC) is also plotted in Fig. 1. The hardness of the CC sample is somewhat lower after the first ARB cycle compared to the RT one, but afterward, it slightly increases up to the 3rd cycle and then decreases during the 4th cycle. In the initial cycle, the hardness is increased due to an important strain hardening and increase of the dislocation density. The slight increase in hardness in the following cycles in the CC sample can be attributed

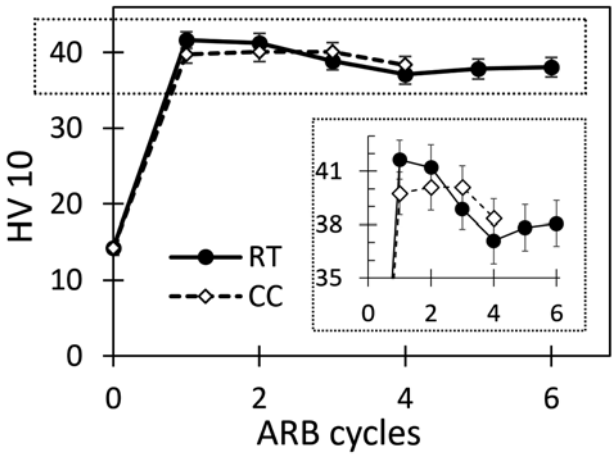

Fig. 1. Hardness evolution during ARB processing at room temperature (RT) and in cryogenic conditions (CC). The inset shows a zoom of the part of the plot in the frame around 40 HV10.

to grain refinement (Fig. 2), moderated by easy recovery and boundary migration in the high purity material without any obstacles. Starting from the 4th cycle in the CC sample and from the 2nd cycle in the RT sample, the recovery processes prevail, and the hardness of the material decreases. On the other hand, if the aluminium matrix contains impurities (e.g., Fe, Si, Cu [18–21]), the movement of dislocations and boundaries is hindered, and so the hardness of the ARB processed Al sheets continues to increase with a slight slope starting from the 2nd ARB cycle due to grain refinement [18–21].

3.2. Grain structure (EBSD)

The grain size of the recrystallized sheet in the initial condition is relatively coarse (in average 71.4 and 53.2 μm in the rolling and normal direction, respectively) and inhomogeneous, because the microstructure of the material does not contain any particles nor foreign atoms in solid solution to hinder the motion of

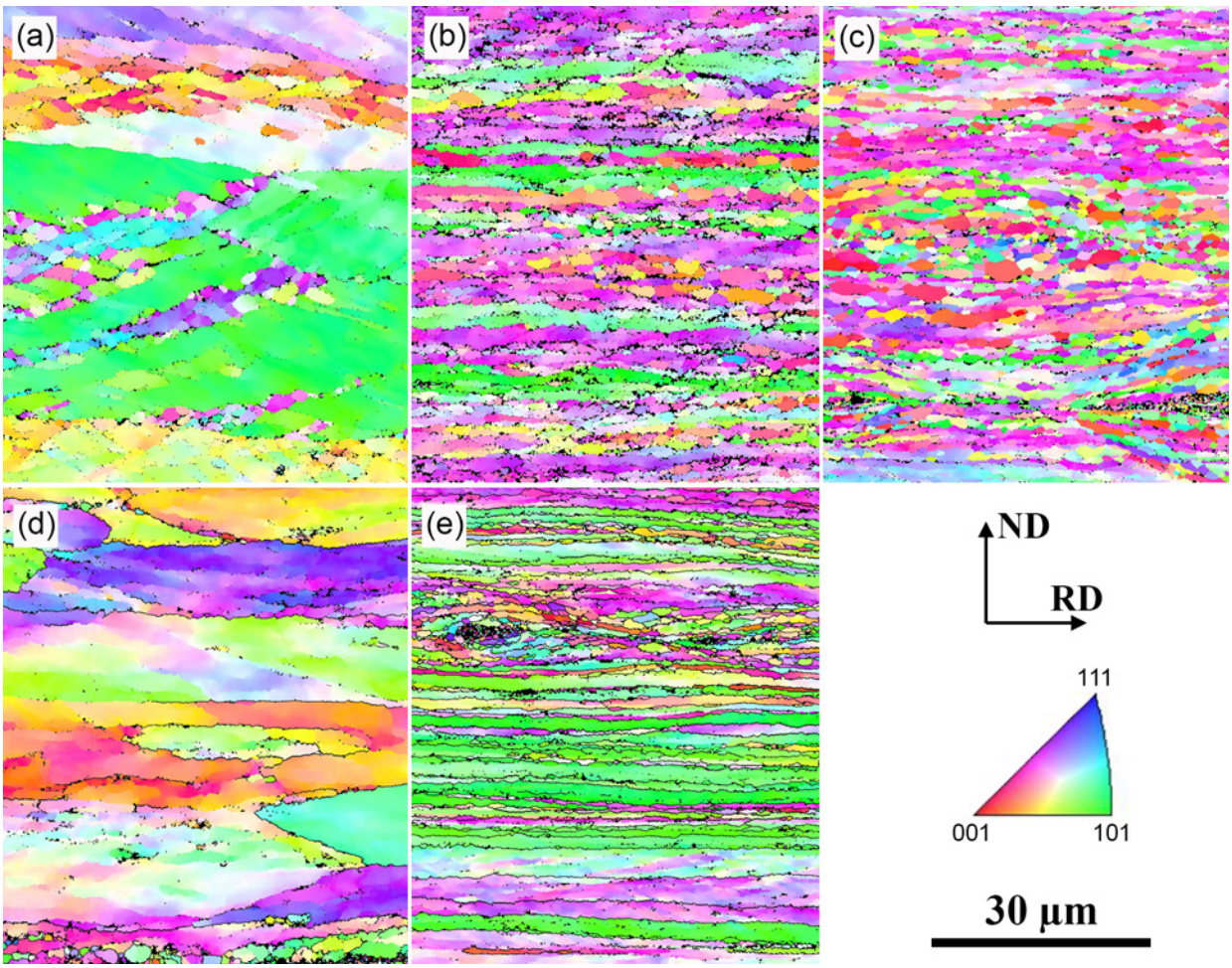

Fig. 2. EBSD orientation maps of the samples of pure Al ARB processed at room (a, b, c) and cryogenic (d, e) temperatures (dark lines in d,e mark HAGB > 15°) by 2 (a, d), 4 (b, e), and 6 (c) cycles.

subgrains and grain boundaries during annealing. The evolution of the grain structure during ARB processing is presented in Fig. 2.

After the 2nd ARB cycle, there are numerous low-angle grain boundaries (LAGB) delimiting cells and subgrains (misorientation angle θ between 2° and 15° – Figs. 2a,d) inside the grains ($\theta > 15°$) of the RT and CC samples. The subgrains are grouped in two categories of bands: deformation bands (inside the grains) and shear bands (intersecting more neighbouring grains). These bands manifest localization of the deformation. With increasing strain due to a higher number of ARB cycles, the high-angle grain boundaries (HAGB) reorient to the direction of rolling, and a lamellar grain structure is formed (Figs. 2b,e). The distance of HAGB in the normal direction (ND) decreases, and this distance approaches the size of subgrains. HAGB represent geometrically necessary boundaries (GNB). Simultaneously, the size of the grains in the rolling direction decreases due to their sectioning by boundaries. These boundaries in the ND are of two types: incidental dislocation boundaries (IDB – LAGB) and GNB (HAGB). The transformation of IDB to GNB (LAGB to HAGB) is provoked by a high strain increasing the stored deformation energy, which is, in turn, a driving force of the reordering of dislocations and dislocation walls into energetically more suitable configurations. After 4 ARB cycles at RT, the grains are quite uniform and elongated in the rolling direction (Fig. 2b). In the corresponding CC sample, most of the volume is occupied by very elongated grains, but close to the wire-brushed surfaces of original joined surfaces, we can find regions with small, nearly equiaxed, recrystallized grains (Fig. 2e). The fragmentation of deformed grains in both samples is not pronounced, but the grains in the RT processed sample are shorter in the rolling direction than in the CC sample. Even after 6 ARB cycles at RT, relatively long grains are still present in the microstructure (Fig. 2c). Incomplete fragmentation is due to the absence of second phase particles acting as obstacles able to pin the boundaries. In consequence, the transformation of LAGB to HAGB is restricted by dynamic recovery. The evolution of the changes in the distance between the grain boundaries l_{ND} in the normal direction from EBSD data is summarized in Table 1. EBSD analysis confirmed that post-deformation recrystallization occurred in the extremely deformed surface layers. The stored energy of cold work in these regions is higher than in the middle of the sheets because there is a superposition of the deformation induced by friction (wire brushing of the surface) and compression plain strain involved in rolling. Both examined ARB cycles led to a more pronounced grain refinement at RT (Table 1, Figs. 2a,b,d,e), both for LAGB $< 5°$ and HAGB $> 15°$ misorientation grain boundaries. The distribution of misorientations of the grain boundaries in CC and RT samples does not differ significantly, and only the CC sample has a little higher fraction of the LAGB with misorientation 2° –5° (histograms not shown here). The fraction of HAGB ($> 15°$) is practically the same for RT and CC samples, the increase of the fraction of LAGB (2° –5°) is at the expense of LAGB (5° –15°) (Fig. 3).

Table 1. Average distance in normal direction l_{ND} between boundaries during ARB

ARB temperature	CC		RT	
Number of ARB cycles	2	4	2	4
l_{ND} (LAGB $< 5°$; (μm))	2.53	0.69	1.36	0.60
l_{ND} (HAGB $> 15°$; (μm))	3.17	0.77	1.60	0.69

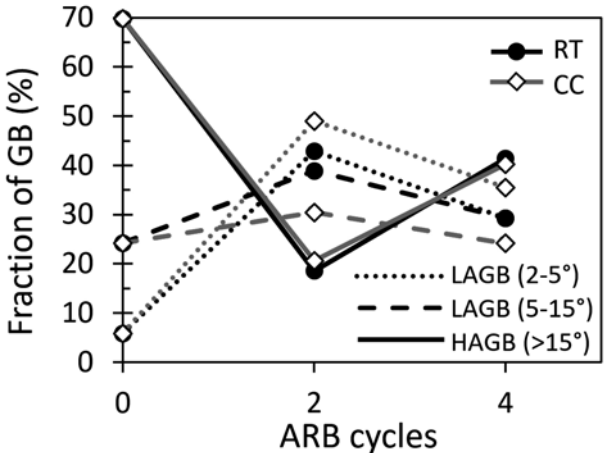

Fig. 3. Changes of the fraction of low- (LAGB) and high-angle (HAGB) boundaries of (sub)grains during ARB processing at room temperature (RT) and in cryogenic conditions (CC).

A similar microstructure was found by Kamikawa et al. [12, 22], who also studied ARB processing of highly pure (99.99 wt.%) Al sheets. Employing TEM, they found HAGB spaced 0.69 μm in the normal direction after 6 ARB cycles at RT. This corresponds to our value after 4 cycles from EBSD analysis (Table 1). Values for 99.99 % Al are somewhat larger than typical values of 0.2–0.3 μm reported for lower commercial purity Al sheets ARB processed to high strain [18–20]. Wang et al. report normal direction average boundary spacing of 0.6 μm after 2 ARB cycles and 0.43 μm after 4 ARB cycles in Al 99.6 wt.% processed in cryogenic conditions [21]. This grain refinement is more pronounced in comparison with our corresponding values of 3.17 and 0.77 μm for HAGB (Table 1) due to impurities that impede grain boundary migration.

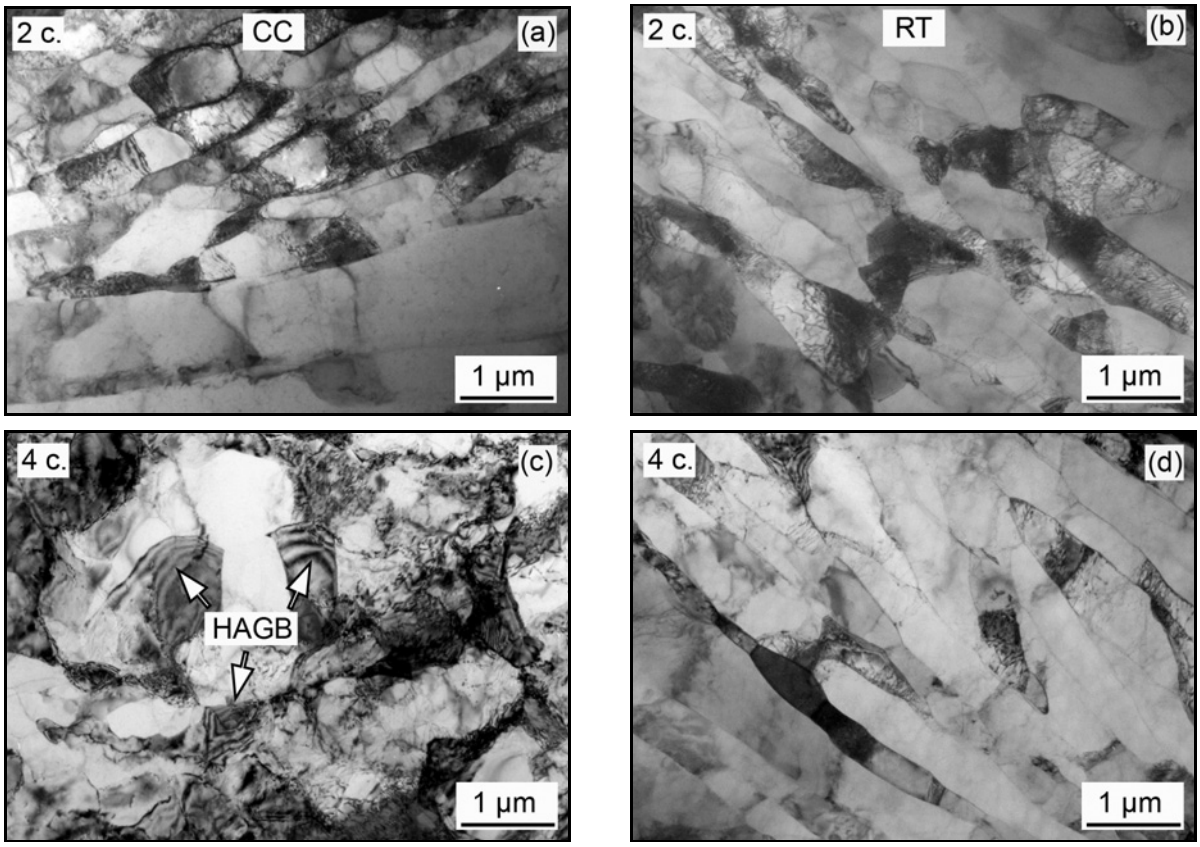

Fig. 4. Transmission electron micrographs of the pure Al sheet ARB processed by two cycles (a, b), and four cycles (c, d) at cryogenic (a, c) and room (b, d) temperature (view in the direction T); arrows in (c) point to recrystallized grains with high-angle (HAGB) boundaries.

3.3. Substructure (TEM)

In TEM, (high-angle, $\theta > 15°$) grain boundaries appear in a typical fringe contrast (marked by arrows in Fig. 4c) if inclined to the electron beam. Subgrain boundaries are often constituted of arrays or networks of dislocations. The neighbouring subgrains have a low misorientation (even $< 2°$), and so they appear together in the diffraction contrast (close to the Bragg condition). TEM observations revealed lamellar grains of sub-micrometer size in both samples processed by two ARB cycles (Figs. 4a,b). In the CC sample, the subgrains forming lamellae have a length in the range from 0.75 to 2 μm and thickness from 0.3 to 1.5 μm (Fig. 4a). In some regions of the CC sample, there were recrystallized grains, and low-angle twist grain boundaries (LAGB) constituted of regular arrays of dislocations. In other regions in the volume, there were dislocations arranged in dislocation cells. The RT sample showed a similar substructure, but a more detailed comparison showed that the subgrains in the CC sheet after 2 ARB cycles were much bigger than in the sample processed at RT (Figs. 4a,b). This is due to more pronounced post-deformation softening processes (recovery and partial recrystallization) in the CC samples. A more intensive softening process can be ascribed to the higher stored energy of cold working in CC sheets because the dynamic recovery is lower in the CC than in the RT samples. Dynamic recovery is connected with the thermally activated dislocation movement, which is less probable at CC than at RT. In the samples processed by 4 ARB cycles, the difference was even more pronounced. In the CC sample, there were very fine and equiaxed subgrains, dislocation cells and in several places also recrystallized grains with HAGB (marked by arrows in Fig. 4c). The number of recrystallized grains is higher after 4 ARB cycles than after 2 ARB cycles. On the other hand, the corresponding RT sample showed a recovered lamellar structure (Fig. 4d). The size of the subgrains and cells in the CC sample is approximately 1 μm, while the thickness of the lamellae in the RT sample is about 0.5 μm. Our results agree with Wang et al. [21], who studied ARB processing of 99.6 wt.% Al sheet up to five cycles in cryogenic conditions.

4. Conclusions

Pure aluminium sheets (99.99 wt.% Al) were pro-

cessed by accumulative roll-bonding (ARB) at room temperature (RT) and in cryogenic conditions (CC). A significant hardening of the material was observed only after the first ARB cycle, the following cycles for the CC sample were accompanied by a small increase of hardness up to the 3rd cycle, while the RT sample slightly softened starting from the 2nd ARB cycle. ARB processing led to significant grain refinement; more refined grains were found in the RT sample, both for $< 5°$ and $> 15°$ misorientation grain boundaries. The distribution of misorientations of the grain boundaries in CC and RT samples does not differ significantly; only the CC sample has a little higher fraction of the LAGB with misorientation 2°–5° at the expense of LAGB (5°–15°). A more intensive softening process can be ascribed to the higher stored energy of cold working in CC sheets because the dynamic recovery is lower in the CC than in the RT samples.

Acknowledgement

This research was financially supported by ERDF in the frame of the project "Nanomaterials center for advanced applications", No. CZ.02.1.01/0.0/0.0/15_003/0000485.

References

[1] N. Hansen, Hall-Petch relation and boundary strengthening, Scripta Materialia 51 (2004) 801–806. doi:10.1016/j.scriptamat.2004.06.002

[2] M. A. Meyers, A. Mishra, D. J. Benson, Mechanical properties of nanocrystalline materials, Progress in Materials Science 51 (2006) 427–556. doi:10.1016/j.pmatsci.2005.08.003

[3] R. Z. Valiev, T. G. Langdon, Principles of equal-channel angular pressing as a processing tool for grain refinement, Progress in Materials Science 51 (2006) 881–981. https://doi:10.1016/j.pmatsci.2006.02.003

[4] Y. T. Zhu, T. Zhua, T. G. Langdon, Performance and applications of nanostructured materials produced by severe plastic deformation, Scripta Materialia 51 (2006) 825–830. doi:10.1016/j.scriptamat.2004.05.006

[5] H. Gleiter, Nanocrystalline materials, Progress in Materials Science 33 (1989) 223–315. doi:10.1016/0079-6425(89)90001-7

[6] N. Y. C. Yang, T. J. Headley, J. J. Kelly, J. M. Hruby, Metallurgy of high strength Ni-Mn microsystems fabricated by electrodeposition, Scripta Materialia 51 (2004) 761–766. doi:10.1016/j.scriptamat.2003.11.001

[7] R. Z. Valiev, R. K. Islamgaliev, I. V. Alexandrov, Bulk nanostructured materials from severe plastic deformation, Progress in Materials Science 45 (2000) 103–189. doi:10.1016/S0079-6425(99)00007-9

[8] R. Z. Valiev, T. G. Langdon, Principles of equal-channel angular pressing as a processing tool for grain refinement, Progress in Materials Science 51 (2006) 881–981. https://doi:10.1016/j.pmatsci.2006.02.003

[9] A. M. Gupta, T. S. Maddukuri, S. K. Singh, Constrained groove pressing for sheet metal processing, Progress in Materials Science 84 (2016) 403–462. doi:10.1016/j.pmatsci.2016.09.008

[10] Y. Saito, H. Utsunomiya, N. Tsuji, T. Sakai, Novel ultra-high straining process for bulk materials – development of the accumulative roll-bonding (ARB) process, Acta Materialia 47 (1999) 579–583. doi:10.1016/S1359-6454(98)00365-6

[11] S. Mroz, A. Wierzba, A. Stefanik, P. Szota, Effect of asymmetric accumulative roll-bonding process on the microstructure and strength evolution of the AA1050/AZ31/AA1050 multi-layered composite materials, Materials 13 (2020) 5401. doi:10.3390/ma13235401

[12] N. Kamikawa, N. Tsuji, Microstructure and mechanical properties of ARB processed aluminium with different purities, Materials Transactions 57 (2016) 1720–1728. doi:10.2320/matertrans.MH201519

[13] N. Tsuji, Production of Bulk Nanostructured Metals by Accumulative Roll Bonding (ARB) Process, In: B. S. Altan (Ed.), Severe Plastic Deformation, Toward Bulk Production of Nanostructured Materials, Nova Science Publishers, New York 2005, pp. 545–565.

[14] P. Qu, L. Zhou, H. Xu, V. L. Acoff, Microtexture development of niobium in a multi-layered Ti/Al/Nb composite produced by accumulative roll bonding, Metallurgical and Materials Transactions A 45 (2014) 6217–6230. doi:10.1007/s11661-014-2545-1

[15] D. Rahmatabadi, R. Hashemi, B. Mohammadi, T. Shojaee, Experimental evaluation of the plane stress fracture toughness for ultra-fine grained aluminium specimens prepared by accumulative roll bonding process, Materials Science & Engineering A 708 (2017) 301–310. doi:10.1016/j.msea.2017.09.085

[16] D. Rahmatabadi, R. Hashemi, Experimental evaluation of forming limit diagram and mechanical properties of nano/ultra-fine grained aluminium strips fabricated by accumulative roll bonding, International Journal of Materials Research 108 (2017) 1036–1044. doi:10.3139/146.111566

[17] D. Rahmatabadi, A. Shahmirzaloo, M. Farahania, M. Tayyebi, R. Hashemi, Characterizing the elastic and plastic properties of the multi-layered Al/Brass composite produced by ARB using DIC, Materials Science & Engineering A 753 (2019) 70–78. doi:10.1016/j.msea.2019.03.002

[18] M. Delshad Gholami, R. Hashemi, M. Sedighi, The effect of temperature on the mechanical properties and forming limit diagram of aluminium strips fabricated by accumulative roll bonding process, J. Mater. Res. Technol. 9 (2020) 1831–1846. doi:10.1016/j.jmrt.2019.12.016.

[19] K. V. Ivanov, V. E. Ovcharenko, Structural features of ultrafine-grained aluminum processed through accumulative roll bonding providing improved mechanical properties and thermal stability, Materials Science & Engineering A 775 (2020) 138988. doi:10.1016/j.msea.2020.138988

[20] L. Su, Ch. Lu, H. Li, G. Deng, K. Tieu, Investigation of ultrafine grained AA1050 fabricated by accumulative roll bonding, Materials Science & Engineering A 614 (2014) 148–155. doi:10.1016/j.msea.2014.07.032

[21] Z. J. Wang, M. Ma, Z. X. Qiu, J. X. Zhang, W. C. Liu, Microstructure, texture and mechanical properties of

AA1060 aluminum alloy processed by cryogenic accumulative roll bonding, Materials Characterization 139 (2018) 269–278. doi:10.1016/j.matchar.2018.03.016

[22] N. Kamikawa, X. Huang, N. Tsuji, N. Hansen, Strengthening mechanisms in nanostructured high-purity aluminium deformed to high strain and annealed, Acta Materialia 57 (2009) 4198–4208. doi:10.1016/j.actamat.2009.05.017